Potential energy surfaces of Polonium isotopes

2015 Phys. Scr. 90 114010

(http://iopscience.iop.org/1402-4896/90/11/114010)

IOP Publishing | Royal Swedish Academy of Sciences Physica Scripta

Phys. Scr. **90** (2015) 114010 (8pp) doi:10.1088/0031-8949/90/11/114010

Potential energy surfaces of Polonium isotopes

B Nerlo-Pomorska[1], K Pomorski[1], C Schmitt[2] and J Bartel[3]

[1] MCS University, 20031 Lublin, Poland
[2] GANIL, CEA/DSM-CNRS/IN2P3, F-14076 Caen, France
[3] IPHC, UDS-CNRS, F-67037 Strasbourg, France

E-mail: krzysztof.pomorski@umcs.pl

Received 20 October 2014
Accepted for publication 13 January 2015
Published 29 October 2015

Abstract

The evolution of the potential energy landscape is analysed in detail for ten even–even polonium isotopes in the mass range $188 < A < 220$ as obtained within the macroscopic–microscopic approach, relying on the Lublin–Strasbourg drop model and the Yukawa-folded single-particle energies for calculating the microscopic shell and pairing corrections. A variant of the modified Funny–Hills nuclear shape parametrization is used to efficiently map possible fission paths. The approach explains the main features of the fragment partition as measured in low-energy fission along the polonium chain. The latter lies in a transitional region of the nuclear chart, and will be essential to consistently understand the evolution of fission properties from neutron-deficient mercury to heavy actinides. The ability of our method to predict fission observables over such an extended region looks promising.

Keywords: nuclear fission, fission fragment mass distribution, shell effects, macroscopic–microscopic model

1. Introduction

In the uranium region, low-energy fission turns out to be strongly asymmetric. It is by now a well established fact that the asymmetry originates from the influence of shell effects in the nascent fragments (see [1] and references therein). With increasing atomic and mass numbers, symmetry is rather abruptly recovered for the ^{258}Fm fissioning nucleus. Here, again, it is well understood that this is caused by the proximity of a favoured partitioning into two closed shell ^{132}Sn fragments. For elements lighter than uranium, a progressive transition from asymmetric to symmetric splitting was clearly pinned down by the experiment of [2]. The transition was found located around ^{226}Th. Schematically, heavier nuclei at low excitation energies (i.e. low temperatures) fission predominantly asymmetrically, while lighter nuclear systems fission symmetrically. In this context, the recent experimental observation [3] of asymmetric low-energy fission of ^{180}Hg came as a surprise. Indeed, according to the understanding acquired with actinides, it would be anticipated that this nucleus would preferentially split into two shell-stabilized ^{90}Zr fragments. The discovery by Andreyev *et al* [3] triggered a tremendous experimental and theoretical research activity in this region at various laboratories around the world. Most recent measurements corroborated the early finding [3], and firmly established the occurrence of an asymmetric splitting in the neutron-deficient pre-actinide region [4]. Even more interestingly, it suggests the possibility of a transition from asymmetric to symmetric fission for a fissioning mass around $A_{\rm fiss} \approx 204$, similar (but reversed) to the transition observed near $A_{\rm fiss} \approx 226$ in the actinides.

According to the most recent data [4, 5], it seems to be clear now that the competition between predominantly symmetric and asymmetric fission depends on both the atomic number Z and the N/Z ratio of the fissioning system. To further study these dependences, the polonium ($Z = 84$) isotopic chain constitutes a particularly relevant test case, as it is situated mid-way between mercury and the 'traditional' actinides.

Since its discovery 75 years ago, fission has shown to be a particularly complex process, involving several poorly known features. The latter can compensate each other in a

subtle way, yielding an intricate interplay, from which specific aspects are difficult to determine unambiguously. Conclusions on fundamental properties extracted from fission observables can thus be strongly model-dependent. At low temperature, the fission process is mainly governed by static effects, while, at higher excitation energy, stochastic thermal fluctuations start to play an increasingly important role. The foremost ingredient of a model aimed at describing fission at low temperature is thus the potential energy landscape, i.e. the evolution of the potential energy of the fissioning nucleus as function of its shape. It has been demonstrated that any realistic account of the latter requires considering a multi-dimensional (nD) deformation space [6], including the large variety of shapes the system may take along the path from its equilibrium state (characteristic of the compact compound nucleus) towards the scission configuration (characteristic of the specific fragments). While such a description seems, in principle, quite straightforward, it represents, in practice, a very challenging task. To make the calculation tractable, one has to restrict it to a reasonable number n of deformation degrees of freedom, and the computation of the potential energy in each deformation point of the nD grid has to be reasonably fast. These two technical aspects are essential to perform large scale and systematic calculations of fission properties over an extended region of the nuclear chart, and thus uncover the evolution of these properties as a function of fissility and isospin.

We have developed a model matching the above two requirements. It is based on the 4D modified Funny–Hills (MFH) shape parametrization as for the deformation space, and the macroscopic-microscopic method for the calculation of the potential energy using the Lublin–Strasbourg drop (LSD) and the Yukawa-folded (YF) single-particle levels. The model explains quite well the strongly asymmetric fission in uranium, plutonium and the lightest fermium isotopes, and the return to a symmetric fragment mass distribution for the heaviest fermium isotopes [7]. In addition, it properly describes the change from asymmetric to predominantly symmetric splitting with decreasing mass number $A_{\rm fiss}$ along the thorium isotopic chain [8]. Recent investigations show that it also qualitatively explains the above mentioned experimental observation of asymmetric fission in neutron-deficient Hg isotopes [7]. Finally, the model is found to reproduce quite well the experimental macroscopic fission barrier heights, in particular in the Po region of primary interest here [9]. It is thus the goal of the present contribution to apply the LSD+YF model in the MFH space to the polonium isotopic chain. The potential energy landscape is calculated and analysed for ten even–even isotopes between ^{188}Po ($N/Z = 1.24$) and ^{220}Po ($N/Z = 1.62$), allowing covering the isospin range between ^{180}Hg ($N/Z = 1.25$) and ^{238}U ($N/Z = 1.59$) but for an *intermediate* Z number. We look for static fission paths and their evolution along the chain. No dynamical effects are included as a first reasonable approximation to address fission at low temperature.

2. Theoretical model

2.1. Shape parametrization

As mentioned earlier, a nuclear shape parametrization, relevant for the description of the fission process, must be able to account for a huge variety of possible shapes, and, at the same time, it should involve a limited number of degrees of freedom. In the present study, we employ the 4D MFH parametrization [10], which has shown itself to be particularly suited for the description of the fission process. The shape of the deformed nucleus is described in cylindrical coordinates by

$$\rho_s^2(z,\varphi) = \mathcal{N}R_0^2\left(1-u^2\right)\left[1 - B\mathrm{e}^{-(3-B)(u-\alpha)^2}\right]F(\varphi), \quad (1)$$

with

$$F(\varphi) = \frac{1-\eta^2}{1+\eta^2+2\eta\cos(2\varphi)}, \quad (2)$$

where $\rho_s(z,\varphi)$ is the distance of the nuclear surface to the symmetry axis and $u = (z - z_{sh})/z_0$. The elongation of the shape in z-direction is 2 z_0, R_0 is the radius of spherical nucleus, and $\mathcal{N}$ is fixed by volume conservation. The coordinate z_{sh} is defined in such a way that the centre of mass of nucleus is located at $z=0$. The dimensionless parameters $c = z_0/R_0$, B, α and η are the four degrees of freedom of the MHF shapes. They describe, respectively: elongation, neck-constriction, reflection-asymmetry, and non-axiality of the nucleus. Recently, a more efficient grid in the MFH space of parameters was proposed [9, 10] by defining the deformation parameters c and B through new ones called ψ and κ

$$c = 1 + e^{\kappa}\sin\psi, \quad B = 1 - e^{\kappa}\cos\psi. \quad (3)$$

In addition, the left–right asymmetry parameter α was scaled according to $\alpha = \alpha' \exp(-0.7\psi^2)$. As compared to the original (c, B, α, η) deformation set, the (ψ, κ, α', η) ensemble allows one to eliminate deformation points which are far from the fission valley (thus reducing the numerical effort), as well as getting rid of unphysical strongly mass-asymmetric shapes in the scission region. In the present contribution, this last variant of MFH is used to describe the shapes of fissioning nuclei. After having checked that non-axiality does not affect the conclusion of the present work, calculations are restricted to the 3D (ψ, κ, α') deformation space assuming $\eta = 0$ all along. Let us specify here that a spherical shape is obtained for $\psi = \kappa = 0$ (equivalently, $c = 1$, $B = 0$), and that the scission configuration is reached for $\psi = \pi/2$ (equivalently, $B = 1$). We also notice that for small values of ψ, the κ parameter corresponds to the neck degree of freedom, while for ψ values close to scission, a variation of κ affects the elongation of the system [9, 10].

2.2. Macroscopic and microscopic nuclear energy

The total energy $E_{\rm tot}(\psi, \kappa, \alpha', \eta = 0)$ of a nucleus with a given deformation is calculated in the macroscopic-

microscopic approach as

$$E_{\rm tot} = E_{\rm mac} + E_{\rm mic}, \tag{4}$$

where each contribution depends, although not explicitly specified, on the deformation. All details of the calculations are described in [8]. The macroscopic part is calculated within the LSD model [11] which is a liquid-drop type parametrization of the nuclear energy including a curvature term proportional to $A^{1/3}$ in the leptodermous expansion. The LSD prescription has shown to yield a good description of both nuclear ground-state masses and fission-barrier heights. The microscopic part consists of the proton and neutron shell and pairing corrections [8]

$$E_{\rm mic} = E_{\rm shell} + E_{\rm pair} - \left\langle E_{\rm pair} \right\rangle, \tag{5}$$

where $\langle E_{\rm pair} \rangle$ is the average value of the pairing correlations.

For each kind of particle, shell corrections are obtained by subtracting the average energy from the sum of the single-particle (s.p.) energies

$$\mathrm{E}_{\rm shell} = \sum_k e_k - \widetilde{E}. \tag{6}$$

The smooth energy $\widetilde{E}$ is evaluated using the Strutinsky prescription [8, 12]. Pairing corrections are obtained as the difference between the BCS [13] energy and the s.p. energy sum, minus the average pairing energy [13, 18].

$$E_{\rm pair} = E_{\rm BCS} - \sum_k e_k. \tag{7}$$

The s.p. wave functions and s.p. energies e_k are obtained as the eigenstates and eigenvalues of the YF potential [14, 15]. The total energy with its macroscopic and microscopic contributions is calculated on each mesh point of the following grid: ($\psi = -0.3$ to 1.55 with step length 0.05, $\kappa = -0.6$ to 0.6 with step length 0.1, $\alpha' = -0.6$ to 0.6 with step length 0.05). The resulting 3D potential-energy landscape is further analysed throughout the whole deformation space, with special emphasis on the ground state, saddle-point and scission configurations. A minimization with respect to one or the other shape variable is performed to search for possible fission paths.

Our approach has shown itself to be successful in understanding the evolution of the fission mass-partition over a large domain [7, 8]. The relevance of the calculation of the microscopic energy was recently demonstrated in an independent work [16] focusing on the detailed description of fission modes in thorium and uranium nuclei.

3. Results

Motivated by the different behaviour of the fission-fragment mass distribution when going from mercury to heavy actinides, as explained in the introduction, the deformation energy landscape is calculated according to the approach outlined in the previous section for ten even–even polonium isotopes from ^{188}Po to ^{220}Po. As we shall observe below, our calculations predict that symmetric fission dominates along the Po isotopic chain. To start with, we thus consider in figure 1 reflection-symmetric shapes ($\alpha' = 0$). To analyse their respective role, the individual (macroscopic, shell and pairing) contributions to the potential energy are shown in the (ψ, κ) subspace as contour maps for ^{216}Po. The macroscopic energy is normalized to its value for a spherical shape. From the total deformation energy (right lower panel), it is seen that the ^{216}Po nucleus is spherical in the ground state. A secondary minimum is observed at ($\psi = 0.4$, $\kappa = -0.3$), corresponding to a rather compact and slightly necked-in shape (see figure 2 of [9]). The latter is found to be clearly caused by shell corrections (left upper panel). Also, it is observed that shell corrections move the LD saddle point to a more compact shape at ($\psi = 0.8$, $\kappa = -0.2$). Beyond the outer saddle, the fission valley drives the system towards slightly more elongated configurations (corresponding to increasing κ values).

The total deformation energy $\Delta E_{\rm tot}$ in the (ψ, κ) subspace is displayed for the ten isotopes in figure 2. While all are about spherical in the ground state, a marked tendency is observed. When moving away for the magic (N = 126) nucleus ^{210}Po, the landscape becomes very soft, and the secondary minimum around $\psi \approx 0.4$ even practically disappears for the lightest masses.

The LSD+YF estimates for the mass excesses along the Polonium chain are displayed in figure 4 as a function of the mass number, and found to be in good agreement with the experimental data [17] as the rms deviation is 0.46 MeV only. We also show the heights $\mathrm{V_A}$ and $\mathrm{V_B}$ of the inner and outer barrier, as well as the height $\mathrm{V_{II}}$ of the secondary minimum (fission isomeric state). The outer barrier is given with (asy) and without (sym) taking the asymmetry degree of freedom α' into account, illustrating the well-known sizeable impact of reflection-asymmetry, in particular at the second saddle point [18], where that barrier is lowered by as much as 5 MeV around ^{208}Po. All barriers exhibit a maximum in the vicinity of $N = 126$, and steadily decrease when moving away, in accordance with their softer landscape (see figure 2).

The influence of octupole deformation and the possibility of reflection-asymmetric fission is examined in figure 3, where the total deformation energy is shown in the (ψ, α') subspace after minimization with respect to the κ degree of freedom. Again, one notices that with increasing neutron number the landscape exhibits deeper local minima and more pronounced valleys. The latter are observed to be most pronounced around ^{210}Po (N = 126). Yet, in all cases, the symmetric valley is the deepest. In addition, one observes that, from ^{200}Po on, the potential energy surface develops a shallow but quite noticeable local minimum, a couple of MeV deep, that stretches for $\psi \approx 1$ into the asymmetry direction. This minimum, centred at $\alpha' = 0$, is most pronounced for the N = 126 closed-shell isotope, and becomes more shallow

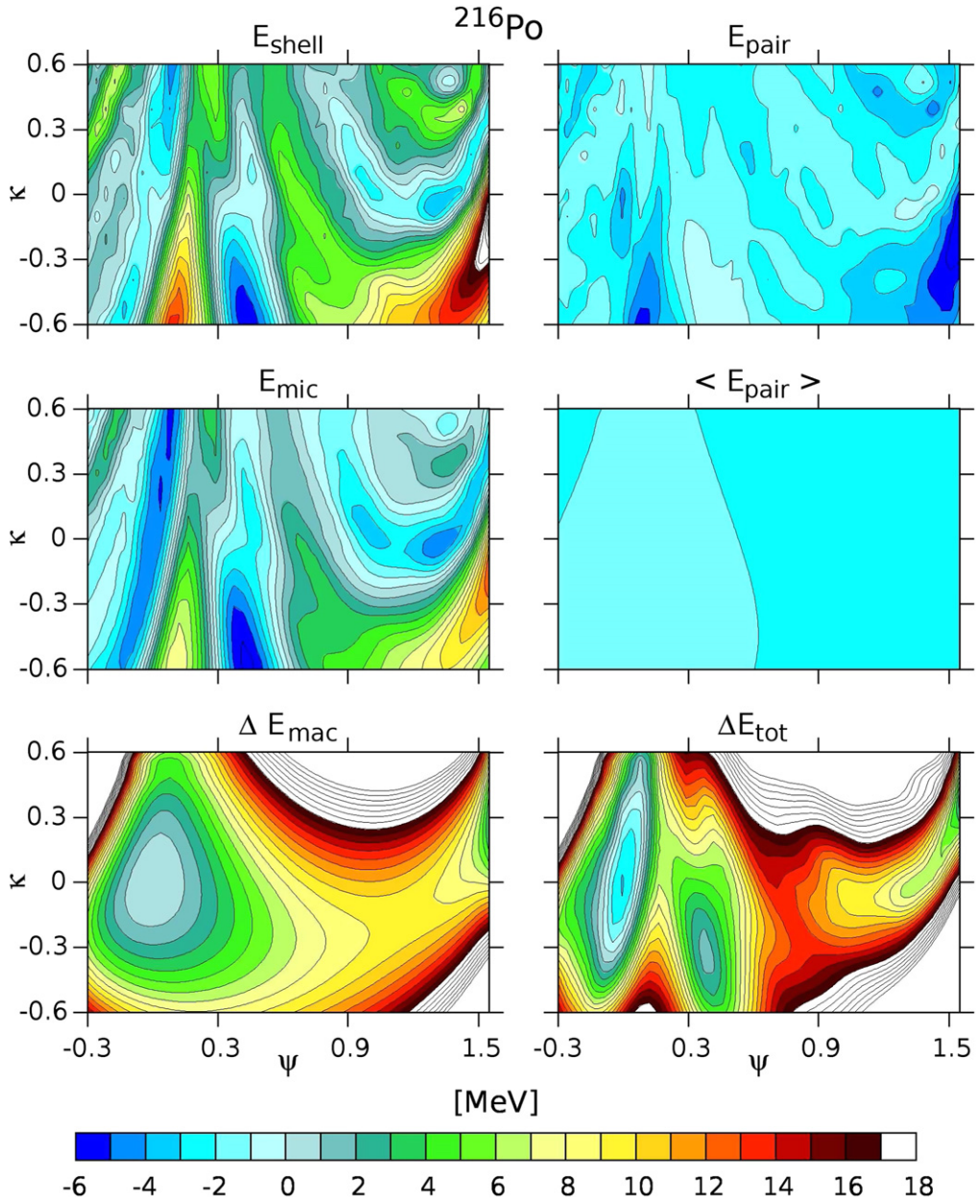

Figure 1. Different contributions to the nuclear energy as obtained in the LSD+YF model for ^{216}Po in the (ψ, κ) deformation space for reflection-symmetric shapes ($\alpha' = 0$). Upper row: total shell correction energy $E_{\rm shell}$ (left) and total pairing energy $E_{\rm pair}$ (right). Middle row: total microscopic correction energy $E_{\rm mic}$ (left) and average pairing energy $\langle E_{\rm pair}\rangle$ (right). Lower row: macroscopic deformation energy $\Delta E_{\rm mac} = E_{\rm mac}(\psi, \kappa, 0, 0) - E_{\rm mac}(0, 0, 0, 0)$ (left) and total deformation energy $\Delta E_{\rm tot} = E_{\rm tot}(\psi, \kappa, 0, 0) - E_{\rm mac}(0, 0, 0, 0)$ (right).

when moving away from shell closure. That suggests that, although symmetric fission prevails for all isotopes, it is predicted to be most favoured and peaked for ^{210}Po, while other isotopes are expected to show a broader fission-fragment mass distribution. These conjectures are in qualitative agreement with the experiment [19] (a more quantitative study is in progress). It is finally worth mentioning that the macroscopic-microscopic landscapes of figure 3 are perfectly in line with the recent self-consistent calculations by McDonnell and co-workers [20].

As a first step in quantifying the above observations, we consider in figure 5 the total deformation energy as a function of asymmetry at constant values of the distance R_{12} between the centres of mass of the two nascent fragments, corresponding basically to cross sections of the landscapes of figure 3 along α'. We restrict this analysis to shapes with ψ beyond $\approx$0.6 for which the system starts developing a neck. The left panel of the upper row illustrates the progressive formation of the symmetric fission valley with increasing R_{12}. The upper right panel shows the dependence

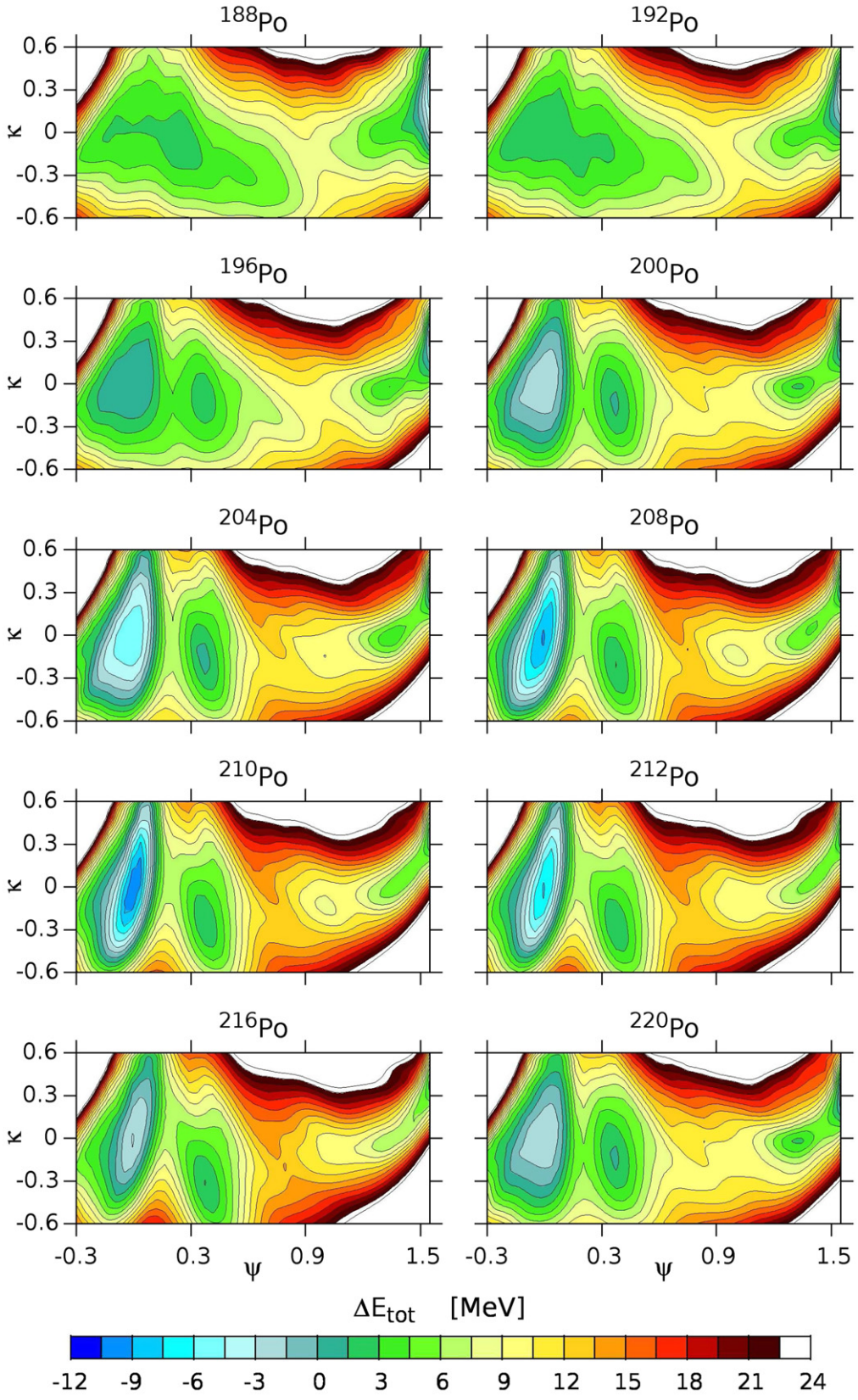

Figure 2. Total deformation energy $\Delta E_{\rm tot}$ in the (ψ, κ) subspace $(\alpha' = 0)$ for ^{188}Po to ^{220}Po.

of the profile of the fission valley along the isotopic chain. According to these curves, the fission-fragment mass distribution of ^{188}Po is expected to be particularly broad, with most probably a flat top. The distribution is predicted to become more and more peaked at symmetry with increasing $A_{\rm fiss}$, and its width to be most narrow at $N = 126$. Beyond

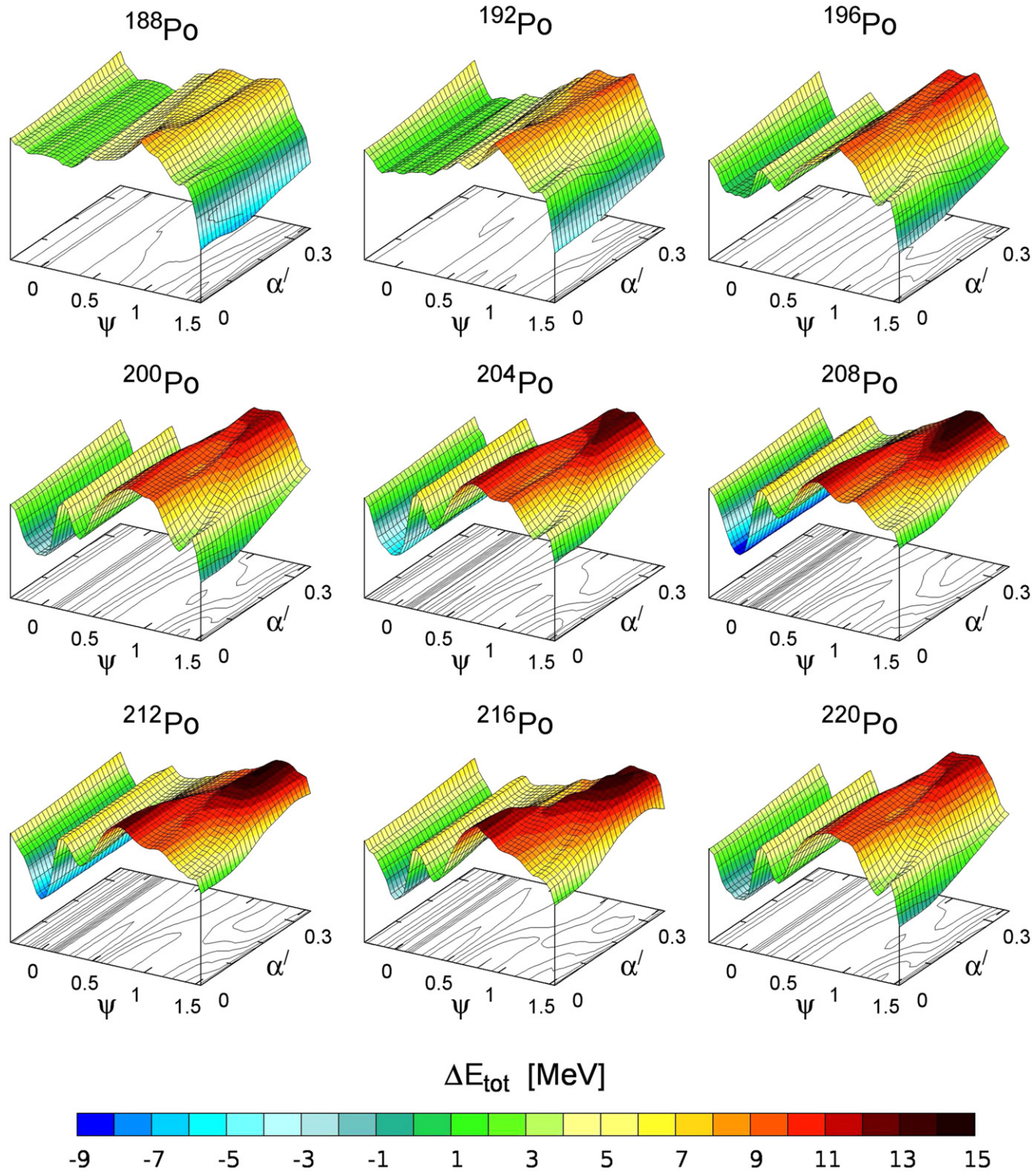

Figure 3. Total deformation energy $\Delta E_{\rm tot}$ in the (ψ, α') subspace for ^{188}Po to ^{220}Po after minimization with respect to κ.

shell closure, the mass distribution is expected to widen again. These predictions are consistent with the few experimental mass distributions (lower panel of figure 5 taken from [19]). They are also in line with the results obtained by other theoretical approaches [21, 22] for the lightest Hg isotopes, which are expected to exhibit a broad fragment mass distribution. In contrast, an asymmetric division is predicted with increasing $A_{\rm fiss}$ along the Hg chain, while we predict that symmetric splitting remains favoured for the heavier Po isotopes. There is also a vivid

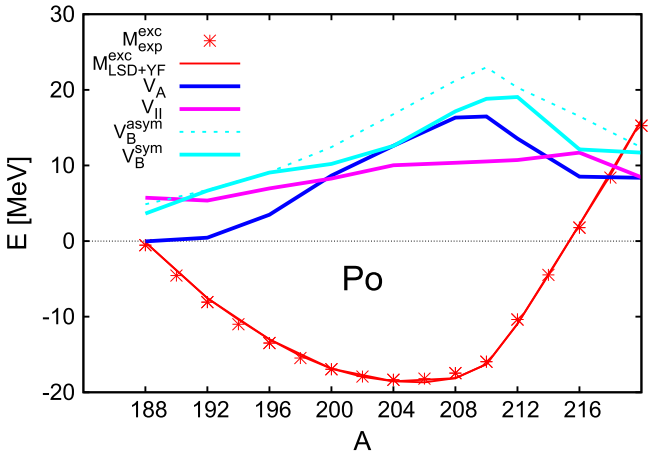

Figure 4. Mass excesses, theoretical M^{exc}_{LSD+YF} and experimental M^{exc}_{exp}, and barrier heights V_A, V_{II}, V_B^{sym} and V_B^{asy} of ^{188}Po to ^{216}Po isotopes.

debate about the evolution of the fragment-mass distribution with A_{fiss} and the excitation energy of Hg isotopes [21, 22], as well as about the very origin of asymmetric splitting [23–25]. The polonium isotopic chain might be worth investigating both theoretically and experimentally, as it may show both similarities and differences with mercury, as our calculations suggest, and thus help understanding mass division in this region [20].

4. Conclusions and perspectives

Within a theoretical approach that combines the efficient MFH parametrization of nuclear shapes and the macroscopic–microscopic method together with the LSD mass formula and the YF single–particle energies, we have analysed the multi-dimensional potential energy landscape of ten even–even polonium isotopes. Equilibrium and saddle-point location were identified, and the favourable fission paths were determined. Our model predicts that symmetric fission dominates over the whole range from ^{188}Po to ^{220}Po with, however, a fission-fragment mass distribution width which strongly depends on the isotope. In particular, this width is expected to be smaller close to the $N = 126$ magic shell. This prediction is in agreement with the experimental data, even though these are limited to three fissioning nuclei. The predictions by our work present also similarities with results obtained by other theories for the Hg chain. However, according to our calculations, the properties of low-energy fission of Hg and Po start to deviate from each other with increasing A_{fiss}. Our model namely predicts that the fragment mass distribution remains peaked at symmetry for the polonium isotopes. It would therefore be particularly interesting to invest experimental efforts in measuring the fission properties of the Po chain, as they may help to map the fissility and isospin dependence in the transitional region between mercury and heavier actinides. Additionally, the fission properties of this chain have the advantage of being more easy to access in experiment owing to the larger fissility of Po as compared to Hg.

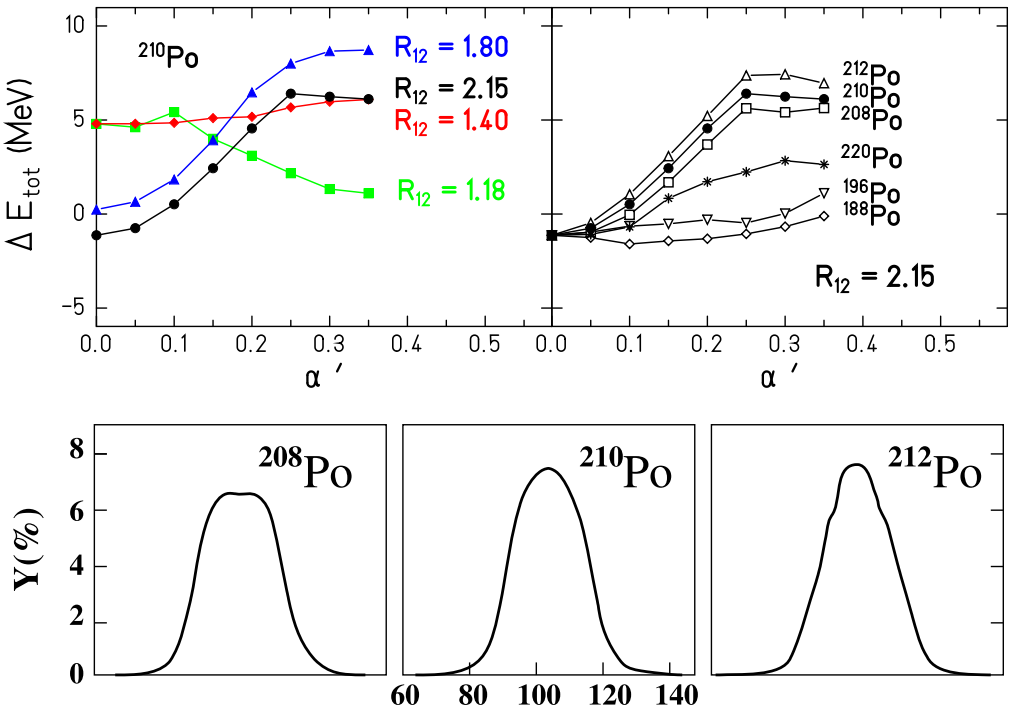

Figure 5. Upper row: left: total deformation energy ΔE_{tot} of ^{210}Po as function of reflection-asymmetry for various distances R_{12} (in units of R_0) between the centre of mass of the nascent fragments. Right: total deformation energy ΔE_{tot} as function of reflection-asymmetry of ^{188,196,208,210,212,220}Po close to scission ($R_{12} \approx 2.15$). To ease comparison, all energies have been normalized to that of ^{210}Po for $\alpha' = 0$. Lower row: experimental fragment mass distribution for fission of ^{208,210,212}Po [19] at about 10 MeV excitation energy.

Acknowledgments

This work has been partly supported by the Polish–French COPIN-IN2P3 collaboration agreement under project number 08–131 and by the Polish National Science Centre, grant no. 2013/11/B/ST2/04087.

References

[1] Schmidt K H 2011 *Lecture Notes Ecole Joliot Curie* http://ejc2011.sciencesconf.org/resource/page?id=28
[2] Schmidt K H *et al* 2000 *Nucl. Phys.* A **665** 221
[3] Andreyev A N *et al* 2010 *Phys. Rev. Lett.* **105** 252502
[4] Andreyev A N 2013 INT Program 13-3 on quantitative large amplitude shape dynamics: fission and heavy ion fusion http://int.washington.edu/talks/WorkShops/int133/People/AndreyevA/Andreyev.pdf
[5] Gorbinet T 2014 *Scientific Workshop on Nuclear Fission dynamics and the Emission of Prompt Neutrons and Gamma Rays (Opatija, Croatia, September 2014)*
[6] Moeller P *et al* 2001 *Nature* **409** 785
[7] Nerlo-Pomorska B *et al* 2014 *Phys. Scr.* **89** 054031
[8] Nerlo-Pomorska B *et al* 2013 *Phys. Scr.* T **154** 014026
[9] Bartel J *et al* 2015 *Phys. Scr.* **90** 114004
[10] Bartel J *et al* 2014 *Phys. Scr.* **89** 054003
[11] Pomorski K and Dudek J 2003 *Phys. Rev.* C **67** 044316
[12] Strutinsky V M 1967 *Nucl. Phys.* A **95** 420
[13] Nilsson S G *et al* 1969 *Nucl. Phys.* A **131** 1
[14] Davies K T R and Nix J R 1976 *Phys. Rev.* C **14** 1977
[15] Dobrowolski A 2007 *Phys. Rev.* C **75** 024613
[16] Ryzhov I V *et al* 2011 *Phys. Rev.* C **83** 054603
[17] Wang M *et al* 2012 *Chin. Phys.* C **36** 1603
[18] Moeller P 1972 *Nucl. Phys.* A **192** 529
[19] Mulgin S I *et al* 1998 *Nucl. Phys.* A **640** 375
[20] McDonnell J D *et al* 2014 *Phys. Rev.* C **90** 021302
[21] Moeller P *et al* 2012 *Phys. Rev.* C **85** 024306
[22] Andreev A V *et al* 2013 *Phys. Rev.* C **88** 047604
[23] Ichikawa T *et al* 2012 *Phys. Rev.* C **86** 024610
[24] Warda M *et al* 2012 *Phys. Rev.* C **86** 024601
[25] Panebianco S *et al* 2012 *Phys. Rev.* C **86** 064601